Electronic Supplementary Information 1 (22 Pages, 16 Figures, 10 Tables)

Hierarchical Nanoporous Ge Anodes for Lithium-ion Batteries via Plasma-phase-fabricated Mg_2Ge

Zhen Fan[a], Siobhan C. Stevenson [a], Alexander Mungall[a], Akira Nishio[b], Robert Szczęsny[c], Yan-Gu Lin[d], Mark Chen[e], Wei-Ren Liu[f], Shigeto Okada[b], Duncan H Gregory[a*]

a. WestCHEM, School of Chemistry, University of Glasgow, Glasgow, G12 8QQ, United Kingdom.
b. Institute for Materials Chemistry and Engineering, Kyushu University, 6-1, Kasuga-koen, Kasuga 816-8580, Japan.
c. Faculty of Chemistry, Nicolaus Copernicus University in Toruń, ul. Gagarina 7, 87-100 Toruń, Poland.
d. Research Division, National Synchrotron Radiation Research Center, Hsinchu 30076, Taiwan.
e. Advancharis Co. Ltd., Zhongshan Rd., Zhonghe Dist., New Taipei City 23557, Taiwan.
f. Department of Chemical Engineering, Chung Yuan Christian University, R&D Center for Membrane Technology, Research Center for Circular Economy, 32023, No. 200, Chun Pei Rd., Chung Li District, Taoyuan City 32023, Taiwan.

* Corresponding Author. Duncan.Gregory@glasgow.ac.uk; Tel: +44-141-330-8128.

Description of Supplementary Information Files

1. Documents

Electronic Supplementary Information 1 (pdf) – Documentation of supplementary experimental & analysis details plus supporting figures and tables.

2. Videos

Supporting Video 1 (mkv) – 1st MW irradiation of Mg/GeO_2 at 200 W for 20 s under a static vacuum ($P = 1.0\times10^{-1}$ mbar), movie played at 1× speed with a frame rate of 60 f/s.
Supporting Video 2 (mkv) – 2nd MW irradiation of Mg/GeO_2 at 200 W for 60 s under a static vacuum ($P = 1.0\times10^{-1}$ mbar), movie played at 1× speed with a frame rate of 60 f/s.
Supporting Video 3 (mpg) – Constructed 3D TXM video of a particle of as-synthesised hierarchical nanoporous Ge.
Supporting Video 4 (mkv) – MW irradiation of GeO_2 powders at 200 W for 20 s under a static vacuum ($P = 1.0\times10^{-1}$ mbar), movie played at 1× speed with a frame rate of 29 f/s.

Experimental

Synthesis. 1 mmol GeO_2 powder (Johnson Matthey) and 5.5 mmol Mg powder (99.8%, 325 mesh, Alfa-Aesar) were thoroughly mixed and transferred into a quartz tube. The sample preparation was performed entirely inside a N_2-filled LABstar glovebox (mBRAUN) with H_2O & O_2 concentrations each < 0.5 ppm. The MIMP synthesis was performed using the apparatus illustrated in Scheme S1,[1] by following the procedure below:

(1) Initially the reaction tube was closed using a fitted Polytetrafluoroethylene (PTFE) Young's tap in the glovebox, transferred to a modified single-mode MW reactor (CEM Discovery, 2.45 GHz) and connected to a vacuum line. The 1st MW irradiation was performed using an incident power of 200 W for 20 s under a static vacuum of 1.0×10^{-1} mbar, after which the tube was cooled naturally and the products characterised. **(2)** After grinding the product powders from step 1 in a fume hood, a 2nd MW irradiation was performed using the same set-up, at 200 W for 60 s under a static vacuum of 1.0×10^{-1} mbar. The products were characterised after cooling. (The observations of MIMP synthesis are provided in Supporting Videos 1 and 2.)

Thermal de-alloying and washing steps were performed subsequently in order to obtain pure NP Ge powders. The following procedure was applied: **(3)** The powders from step **2** were thermally dealloyed in air by heating at 550 °C for 11 hours in a box furnace. **(4)** The powders were immersed in 40 mL of 1M HCl aqueous solution for 30 min, centrifuged and washed with deionized water (3 times) and ethanol (3 times), and dried in an oven at 60 °C for 5 h before cooling naturally. NP Ge powders were stored in a N_2-filled glovebox for further tests and characterisation.

In addition to the "deep-reduction" reactions described above, a series of "control" experiments were performed under the same vacuum conditions, in order to obtain experimental evidence towards a further understanding of the MIMP reaction mechanism. In the first of these (**A**), GeO_2 powder was exclusively (i.e. without addition of Mg) irradiated by MWs at 200 W for 20 s. In the second set of experiments, (**B**) approx 2:1 mixtures of Mg:GeO_2 (allowing for a slight excess of Mg) were irradiated as in the Table S1 below. The aim of the **B** experiments was to determine whether GeO_2 could be reduced via the MIMP method directly to Ge without the need to prepare an Mg_2Ge precursor.

Table S1. Experimental parameters for Mg/GeO_2 control experiments; series **B**.

Experiment No.	Amount Mg / mmol	Amount GeO_2 / mmol	MW irradiation cycles #1	#2
i	2.25	1.0	100 W / 30 s	-
ii	2.25	1.0	200 W / 20 s	-
iii	2.25	1.0	200 W / 20 s	200 W / 60 s
iv	2.5	1.0	200 W / 10 s	200 W / 20 s

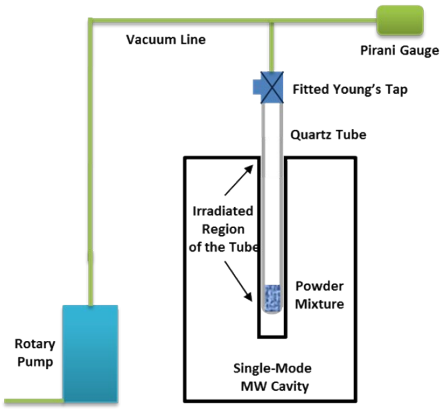

Scheme S1. Experimental setup for the MIMP synthesis.

Electrochemical measurements. The as-synthesised NP Ge powders were mixed with Super P carbon black (99+%, metal basis; Alfa Aesar) and sodium alginate (Sigma Aldrich) binder in a weight ratio of 70:15:15 to form a homogenous slurry. The slurry was coated onto a copper foil (10 microns in thickness) as a current collector and dried at 80 °C for 12 h under a vacuum of 2.0×10^{-2} mbar to fabricate the Ge electrodes. The mass loading of active materials are ~ 0.75-1.10 mg cm^{-2}. Half-cells were assembled using split-able cells (EQ-HSTC-20, MIT) with inner diameters of 20 mm; the Ge electrode (16 mm in diameter) was used as working electrode, a piece of glass fiber/D filter paper (GF/D, 20 mm in diameter; Whatman) soaked with 1.0 M $LiPF_6$ in ethylene carbonate/dimethyl carbonate (EC/DMC, 50/50, v/v; Sigma Aldrich) (*ca.* 0.5 mL for each cell) as the separator. Li foil (99.9%, metal basis, 0.75 mm in thickness; Alfa Aesar) was manually polished and prepared into a clean Li disk (19 mm in diameter) as the counter electrode. All half-cells were assembled in an Ar-filled glovebox with moisture and oxygen levels < 0.5 ppm. Discharge/charge cycles were measured at room temperature using a galvanostatic programmable battery tester (Neware, CT-4008; 5 V 10 mA) at different current densities with a cut-off potential range of 0.05 – 1.00 V. Electrochemical Impedance Spectroscopy (EIS) measurements were performed on cells after battery-cycling at the open-circuit voltage on a Biologic SP-150 potentiostat in the frequency range of 100 kHz to 10 mHz using an amplitude of 10 mV. Once all the electrochemical experiments were completed, the cells were disassembled in the glovebox. The cycled Ge electrode was removed and thoroughly washed with DMC (> 99.5%, anhydrous; Sigma Aldrich), dried under vacuum and stored in the glovebox for further characterisation.

Materials Characterisation. Powder X-ray diffraction (PXD) was performed using a PANalytical X'pert Pro MPD diffractometer in Bragg-Brentano geometry (Cu $K\alpha_1$ radiation λ = 1.5406 Å; accelerating voltage of 40 kV; emission current of 40 mA). Typically, PXD patterns were collected in air at room temperature over a 2θ range of 10−80° with a step size of 0.0334° for 15 min for the rapid phase-identification/matching of the MW-irradiated and thermally-dealloyed powders. One PXD dataset was collected from 10-110° (2θ) with a step size of 0.167° for 2 h in order to perform Rietveld refinement of the structure of the phase-pure NP Ge sample. Rietveld refinement was performed using GSAS via the EXPGUI interface,[2] with a previously published Ge structure taken as an initial crystallographic model.[3] Reported crystallographic structures of GeO_2, Mg_2Ge, Mg and MgO were employed for initial phase identification and then added as impurity phases in Rietveld refinements to obtain precise phase fractions of the products obtained from different

synthesis steps.[4-7] For post-galvanostatic cycling characterisation, powders were peeled off from the cleaned, dry electrode so that PXD measurements could be performed in reflection geometry in airtight sample holders under a protective atmosphere of Ar. Scans were performed for 2 h 10 min over 10-90° (2θ) with a step size of 0.0167°.

Scanning electron microscopy (SEM) and energy dispersive X-ray spectroscopy (EDS) were performed using three instruments: a Philips/FEI XL30 ESEM (beam voltage 20 kV, maximum magnification 20 k) equipped with an INCA X-Act detector (Oxford Instruments Analytical, UK), a Carl Zeiss Sigma Variable Pressure Analytical SEM and a Hitachi S-4100 microscope equipped with an INCA X-Act detector (Oxford Instruments Analytical, UK). The NP Ge sample was coated with either Pt or Au plasma under vacuum to optimise the SEM image quality. For the cycled Ge electrode, the SEM specimen was directly transferred into the SEM instrument without coating in order to keep the air-exposure time < 20 s. Transmission electron microscopy (TEM) and selected area electron diffraction (SAED) of NP Ge powders were analyzed by a TEM microscope (FEI, G2 F20X-Twin 200 kV, FEG) equipped with an energy-dispersive X-ray spectrometer (EDAX, RTEM model SN9577, 134 eV) with measurements performed in the TEM mode (for bright-field imaging). A dispersion of the sample was prepared in ethanol by ultrasound; 5 µl of the solution was dropped onto a Cu TEM grid and stored at room temperature until the solvent had completely evaporated. Post-cycling, the electrode was recovered by disassembling the half-cell in the glovebox before thoroughly washing with DMC (>99.5%, anhydrous, Sigma Aldrich) and drying under vacuum. The dried electrode was cut to prepare specimens for SEM measurements, while powders were peeled from the electrode film for TEM experiments. The respective samples were retrieved from the glovebox in airtight containers and transferred rapidly to the microscopes. It was found that the particles were sensitive to the high-energy electron beam during TEM measurements and TEM images at higher resolution were challenging to obtain.

High resolution Ge*3d* X-ray photoelectron spectroscopy (XPS) was performed using a K-Alpha Photoelectron Spectrometer (monochromatic Al-Kα, Thermo Scientific) under vacuum. Brunauer-Emmett-Teller (BET) analyses were performed on N_2 adsorption-desorption isotherms measured at 77 K (using a Micromeritics TriStar 3000 analyzer). The adsorption data were further analysed using the Barrett-Joyner-Halenda (BJH) method. Samples of *ca*. 150 mg were used for the adsorption-desorption measurements.

Transmission X-ray Microscope (TXM) characterisation was conducted at the beamline station of Taiwan Light Source (TLS 01B1), National Synchrotron Radiation Center (NSRRC) in Hsinchu, Taiwan.[8] The Ge (111) toroidal focusing mirror provided monochromatic light with a photon energy of 8 keV. The transmitted beam passed through a zone-plate and a phase ring to generate an image. The phase ring was positioned at the back focal plane of the zone plate which recorded phase-contrast images at the charge-coupled device (CCD) detector. The beam size for sample observation is about 1 mm × 0.4 mm with an average photon flux of 3×10^{11} photon · sec^{-1} · 200 mA^{-1}. The spatial resolution and field of view of TXM is 50 nm and 15 × 15 μm^2, respectively. TXM 2D tomographic images were collected with a camera binning of 512 × 512 in pixels in the duration of 60 s exposure time. The collected TXM images were further processed and analysed using ImageJ. The Faproma-alignment algorithm was adopted to correct the vertical and rotational motion errors along each projection to improve 3D reconstructed images. In addition, a maximum

likelihood estimation reconstruction method was applied on the 3D image reconstruction using 151 sequential projections along a specific azimuth angle rotation (-90 − 90°). The visible 3D tomographic images and video were reconstructed using Amira 3D image processing software. Quantitative analysis was performed using the Skyscan™ (CT analysis) software package (Bruker), following the transfer of the image set data and the definition of the sample volume (including open pores). Analysis allowed a calculation of the final sample volume, sample area, and the number and volume of open and closed pores (Table S6).

Figures, Tables and additional discussion

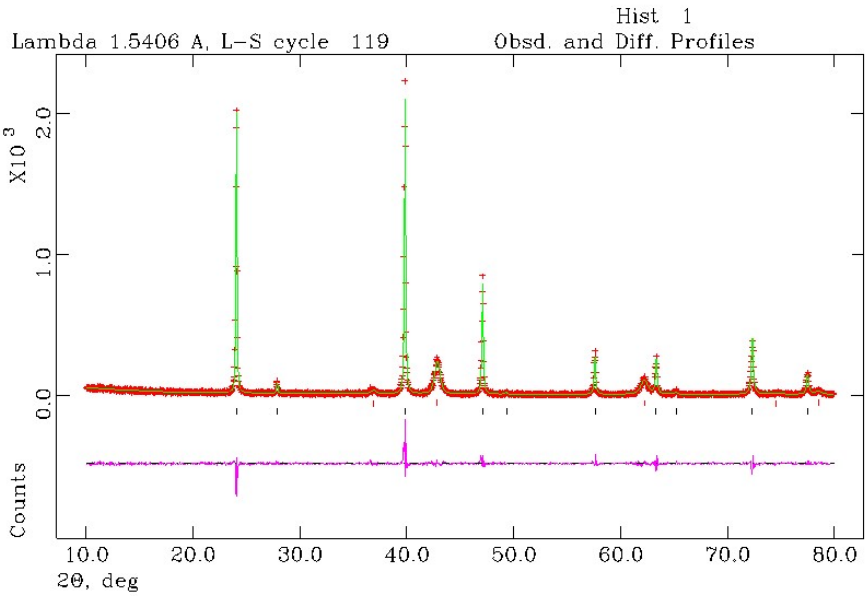

Figure S1. The profile plot from the Rietveld refinement against experimental PXD data of the Mg_2Ge/MgO powder mixture after the 2nd MW irradiation of the 5.5:1 Mg:GeO_2 sample (*i.e.* following a total irradiation time of 80 s; see also Figure 1-ii; Table S8). Red ticks: MgO, black ticks: Mg_2Ge.

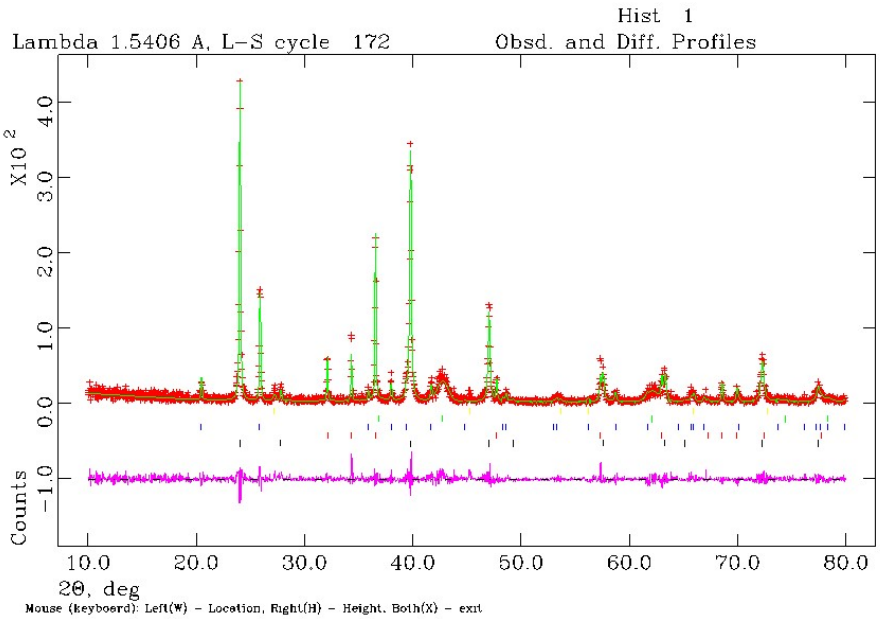

Figure S2. The profile plot from the Rietveld refinement against experimental PXD data of the 5.5:1 Mg:GeO_2 powder mixture after the 1st MW irradiation of 20 s (see also Figure 1-i; Table S9). Red ticks: Mg, black ticks: Mg_2Ge, green ticks: MgO, dark blue ticks: GeO_2, orange ticks: Ge.

PXD results from both "control" experiment sets **A** and **B** are shown in Figure S3. The associated SEM/EDS results are shown in Figures S4 and S5. In the former case (**A**) - and as shown in supporting video 4 - no formation of any plasma occurred for the GeO_2 sample during the first *ca.* 13 s of MW irradiation. The formation of purple plasma in the last *ca.* 7 s likely originates from any gas remaining in the tube following evacuation.[1] Both PXD and SEM revealed that the GeO_2 sample was essentially unchanged both with respect to its composition/crystal structure and in terms of its microstructure (Figures S3, S4). The as-received GeO_2 powder was composed of particles *ca.* 50 μm across, which themselves were composed of agglomerated smaller grains typically of *ca*. 0.3 – 1.5 μm in diameter. This morphology remained following exposure to MWs.

In the second series of experiments (**B**), evidence of reduction to Ge was indeed observed (Figure S3), but regardless of the irradiation conditions, Mg_2Ge was always observed as a by-product, especially following initial irradiation cycles of short duration. The formation of Mg_2Ge under these conditions was perhaps encouraged by the evident Mg plasma phase, which would be able to provide an Mg-rich local environment at the interface with GeO_2 particles. It is possible that longer irradiation times/repeated exposures, perhaps with a smaller molar excess of Mg starting material (i.e. < 2.25:1 Mg:GeO_2), could lead to purer Ge products. However, under the above conditions, the favorable formation of Mg_2Ge could not be completely avoided, leading to the incomplete reduction of the GeO_2 powder. The final product of the 2.25 Mg + 1.0 GeO_2 control experiment **B**-iii in Figures S3 and S5, however, exhibited a different morphology to the as-received GeO_2 powders (Figure S4). The SEM image and corresponding elemental map in Figure S5 indicate that nanoparticles of MgO could be formed at the product surface. A relatively dense distribution of Ge can be observed to the lower-left corner of Figure S5c, suggesting the formation of elemental Ge in this area. The EDS spectrum in Figure S5d showed an Mg : Ge atomic ratio of 43.25 : 12.46, much larger than the nominal 2.25 : 1.0 ratio of starting materials. Such Mg-rich regions at the particle surfaces would indeed indicate the presence of Mg plasma interacting with solid Ge/GeO_2 during the MIMP reaction. Notably, when the Mg amount was increased to 2.5 mmol, PXD results in Figure S3 (B-iv) still suggested incomplete GeO_2 reduction, but with an increasing amount of Mg_2Ge. These kinetically favorable formations of Mg_2Ge instead of Ge probably were not surprising given the ultra-dynamic and locally Mg-plasma-rich environment during the reactions. This indeed benefited the MIMP reaction nominated for the deep reduction of GeO_2 directly to Mg_2Ge with a higher Mg content in the reactants (Scheme 1 and Figure 1 in the main paper).

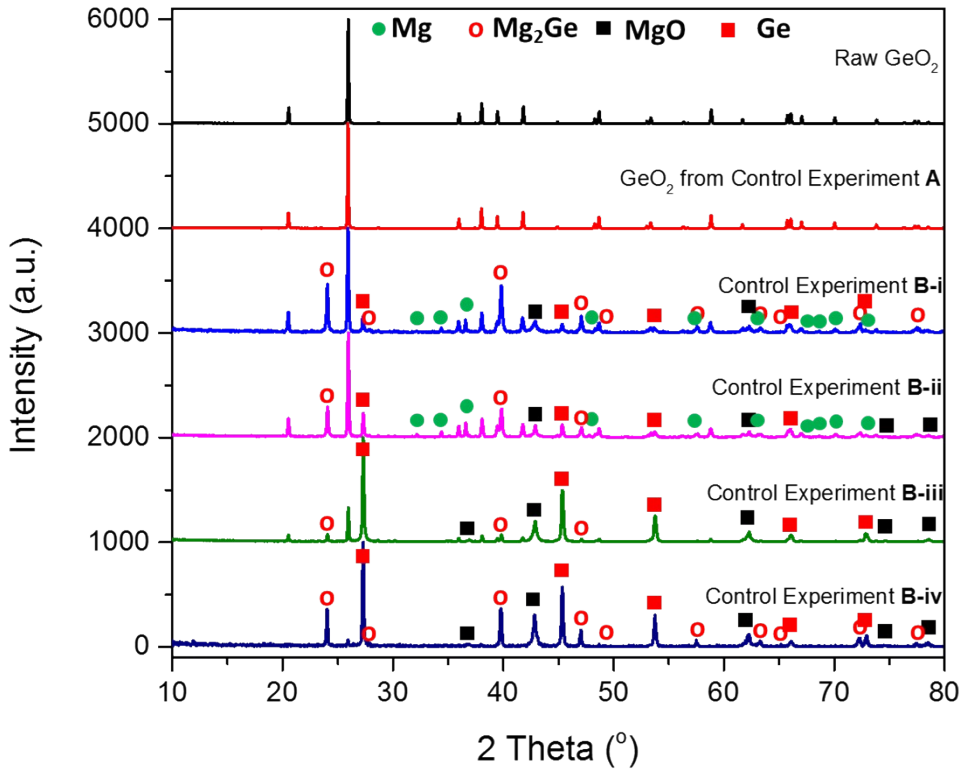

Figure S3. PXD patterns from as-received GeO_2 and from a series of control samples (the respective experimental parameters used are listed in Table S1).

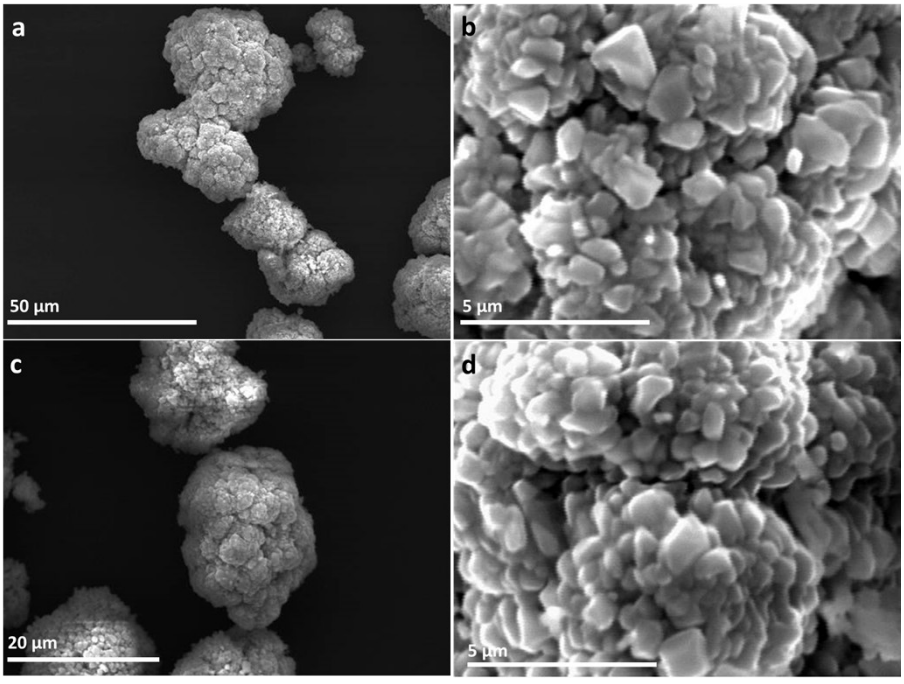

Figure S4. SEM images of **(a, b)** as-received commercial GeO_2 powders and **(c, d)** GeO_2 powders following irradiation by MWs at 200 W for 20 s under a static vacuum 1.0×10^{-1} mbar.

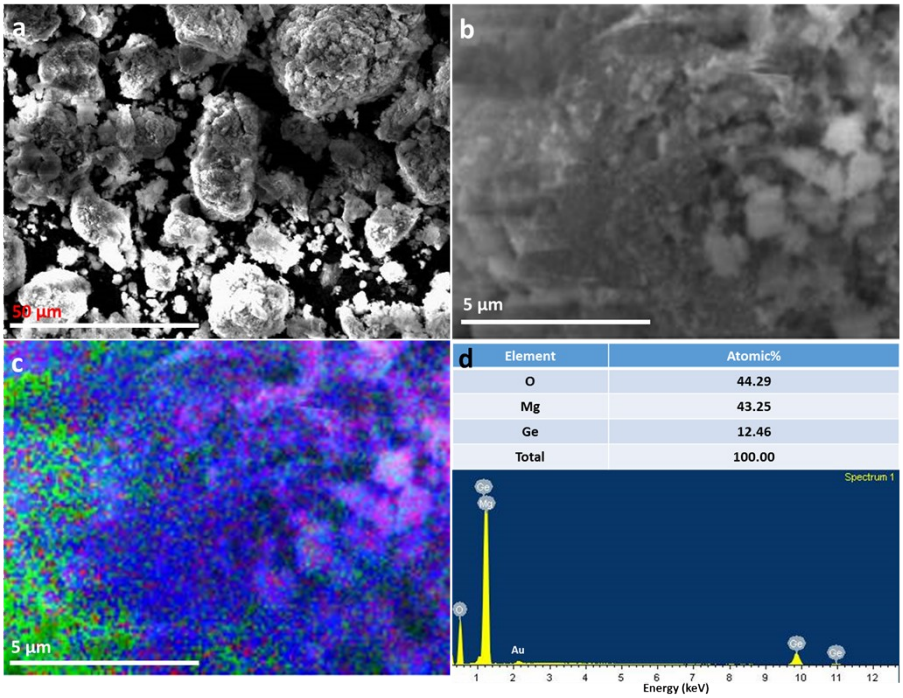

Figure S5. SEM and EDS results of powders from control experiment **B**-iii (Table S1), showing: **(a, b)** SEM images; **(c)** elemental maps of O (Red), Ge (Green), and Mg (Blue) from the image in (b), and **(d)** the corresponding EDS spectrum taken from the entire area shown in (c).

Low magnification SEM images showed that the Mg_2Ge/MgO product generated from the optimised, higher ratio Mg + GeO_2 MIMP syntheses described in the main paper (with the PXD pattern shown in Figure 1-ii) was composed of block-like particles in the micron range (Figure S6a), with a morphology rather different to that of the GeO_2 starting material. At higher magnifications, clusters of nanoparticles of lighter contrast could be observed on and between the larger microcrystalline blocks, which themselves appear to be composed of smaller grains with some level of porosity (Figures S6b,c). Elemental maps indicate that the irregular clusters of smaller particles contain high concentrations of magnesium and oxygen; for example, the finer (nano)particles in the lower-left corner of Figures S6c,d contain principally magnesium and oxygen, implying the presence of MgO. By contrast, only Mg and Ge are distributed relatively uniformly in the larger blocks of particles throughout the sample. The corresponding EDS spectrum and analysis (Figures S6e,f) suggests an Mg : Ge atomic ratio of *ca*. 4.7:1, across the area of the sample, which is close to the ratio of the starting materials used in the initial synthesis.

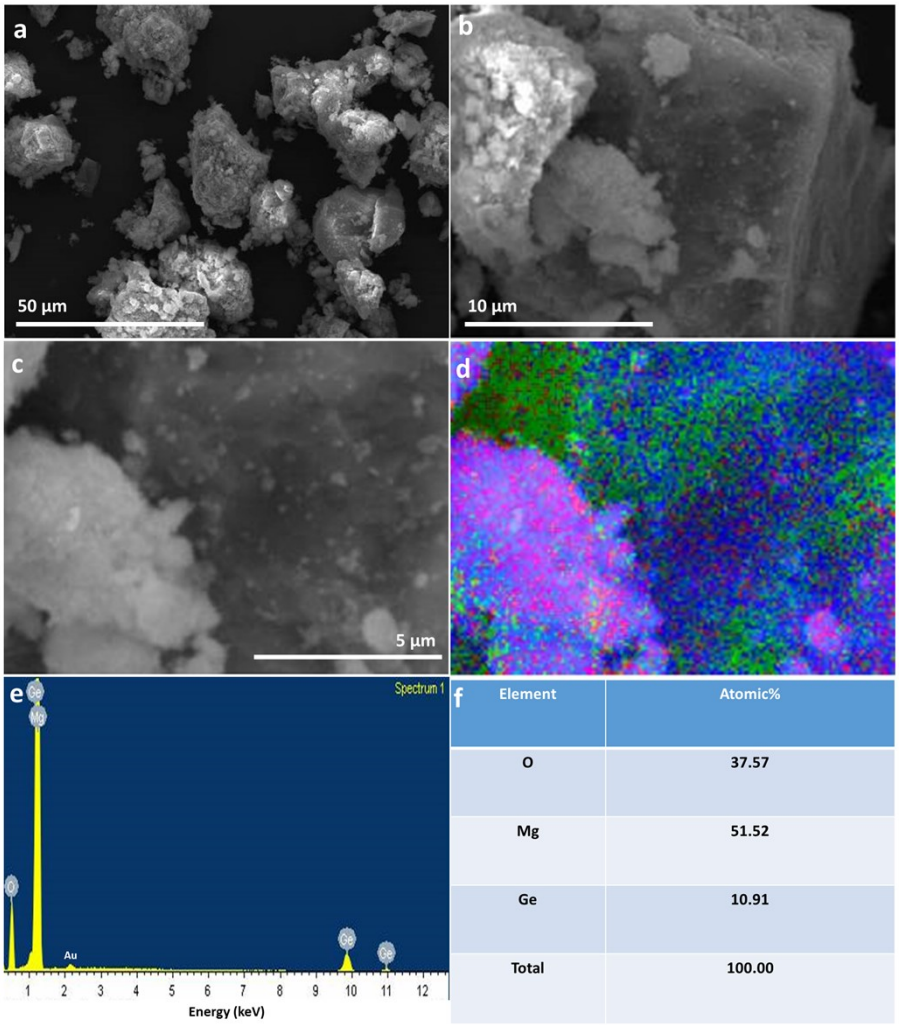

Figure S6. SEM and EDS results of the MIMP-obtained Mg_2Ge/MgO powders in Figure 1c-ii, showing: **(a-c)** SEM images; **(d)** elemental maps of O (Red), Ge (Green), and Mg (Blue) taken from the sample imaged in (c); **(e)** areal EDS spectrum corresponding to the elemental maps in (d) and **(f)** the respective tabulated atomic ratios from the spectrum shown in (e).

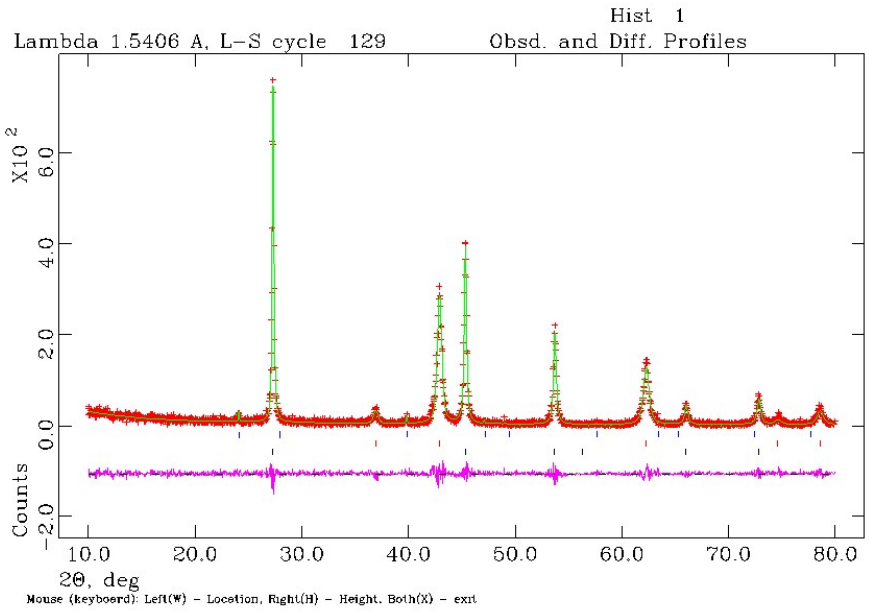

Figure S7. Profile plot from the Rietveld refinement against experimental PXD data of the Mg_2Ge/MgO sample (originally from 5.5:1 Mg:GeO_2) after the thermal de-alloying process and prior to acid washing (see also Figure 1-iii; Table S10). Red ticks: MgO, black ticks: Ge, dark blue ticks: Mg_2Ge.

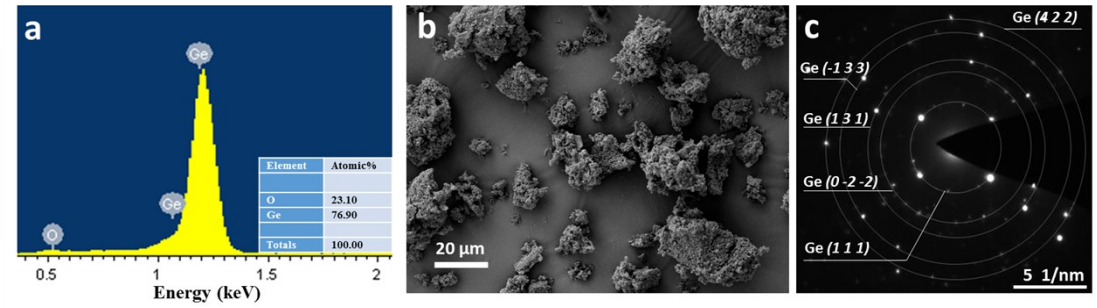

Figure S8. (a) Areal EDS spectrum for NP Ge taken from the area shown in Figure 2b in the main paper; **(b)** a low magnification SEM image of the NP Ge particles, and **(c)** fully indexed version of the SAED pattern of NP Ge presented in Figure 2i in the main paper (see also Table S5 for the list of reflections).

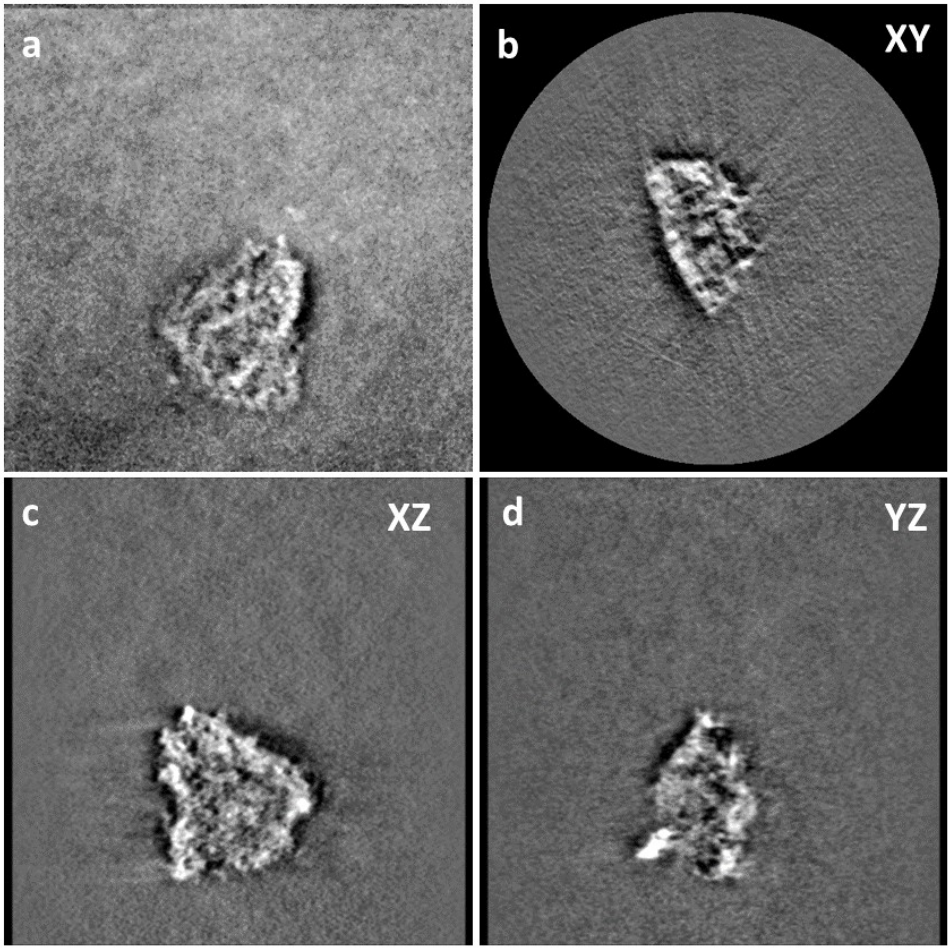

Figure S9. Constructed 3D TXM tomograms showing: **(a)** a raw TXM image and **(b, c, d)** TXM images projected on the three respective axis planes.

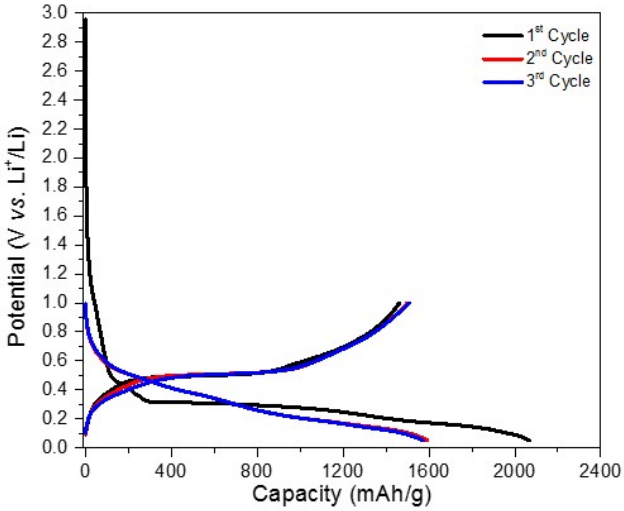

Figure S10. Galvanostatic discharge/charge profiles at 0.16 A g^{-1} (0.1 C) corresponding to Figure 3a.

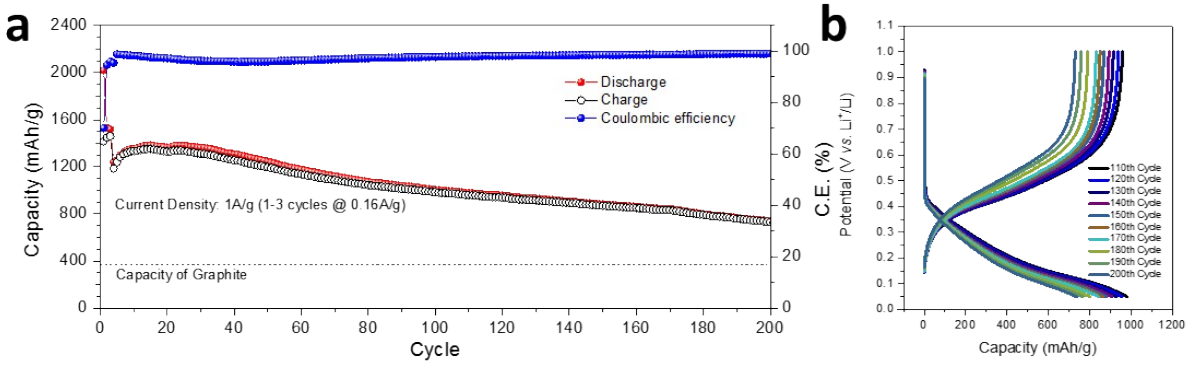

Figure S11. (a) Cycling performance and corresponding coulombic efficiency at 1 A g^{-1} for 200 cycles (first 3 cycles activated at 0.16 A g^{-1}) corresponding to Figure 3e. (The capacity after 200 cycles @ 1A g^{-1} is 736.6 mA h g^{-1}); and **(b)** the respective galvanostatic curves from cycles 100 - 200.

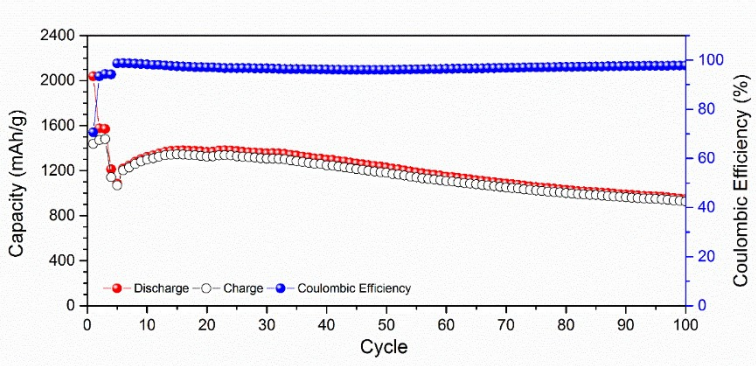

Figure S12. Repeat cycling test at 1 A g^{-1} for 100 cycles (first 3 cycles activated at 0.16 A g^{-1}).

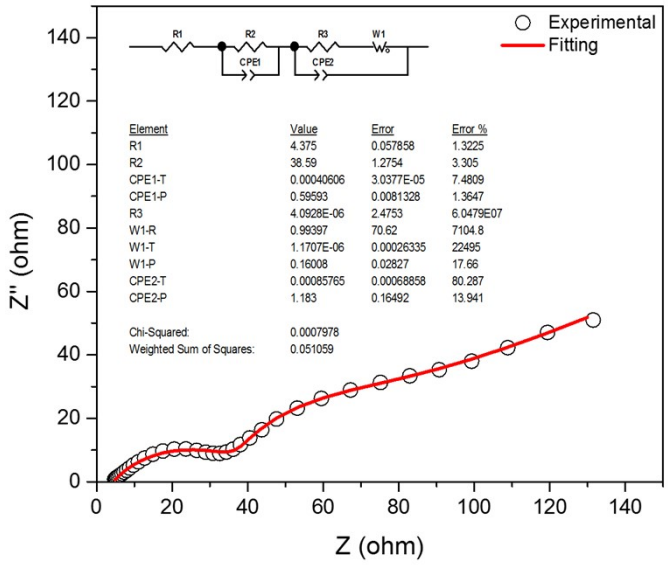

Figure S13. Experimental and fitted EIS spectrum of the cycled cell, tested after the 100 cycles shown in Figure S12. Inset: the equivalent electrical circuit and fitted values for each component.

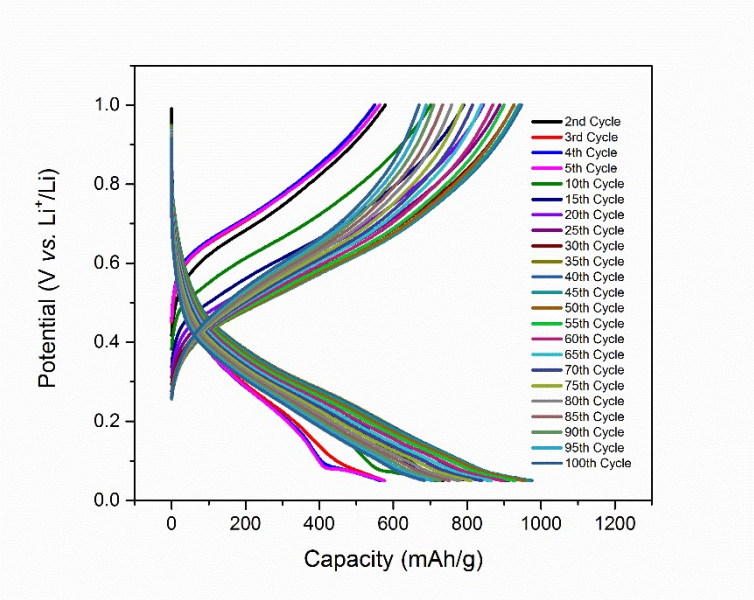

Figure S14. Galvanostatic discharge/charge profiles taken from various cycles for the cycling experiment at 2 A g^{-1} shown in Figure 3e.

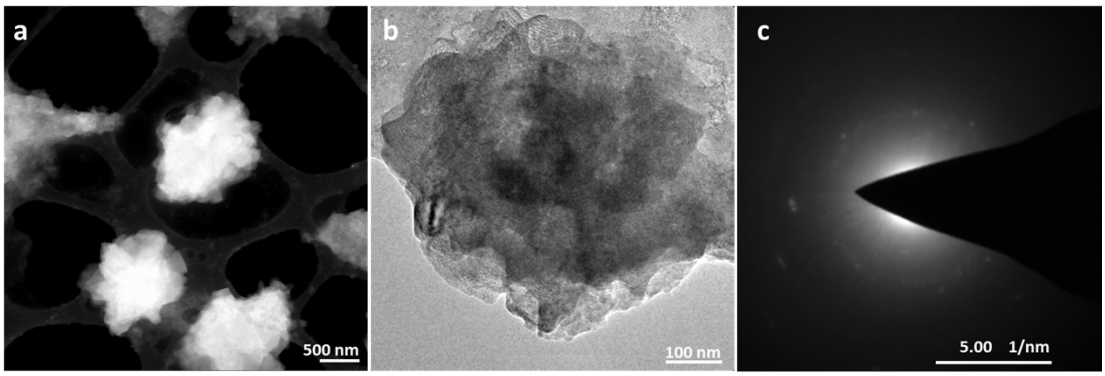

Figure S15. Results from TEM experiments performed on Ge electrode particles after undergoing 200 cycles at 1.0 A g^{-1} as shown in Figure S11, showing: **(a)** High-angle annular dark-field scanning TEM (HAADF-STEM) image of the resulting porous Ge particles; **(b)** TEM image of a cluster of Ge nanograins in close contact, and **(c)** the corresponding SAED pattern from the sample imaged in (b).

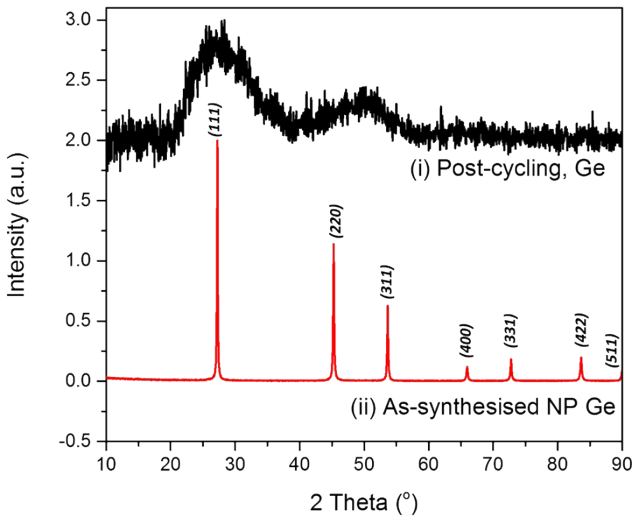

Figure S16. PXD patterns of the post-cycled Ge powders (after undergoing 200 cycles at 1.0 A/g as shown in Figure S11) as compared to the as-synthesised pure NP Ge powders.

Table S2. Crystallographic data obtained from the Rietveld refinement for the as-synthesised hierarchical NP Ge (see also Figure 2a).

Chemical Formula	**Ge**
Crystal System	Cubic
Space Group	*F d -3 m* (N°. 227)
Lattice Parameter, *a* / Å	5.6598(2)
Formula Weight / g mol^{-1}	580.720
Formula Units, *Z*	8
Calculated Density, ρ / g cm^{-3}	5.319
No. of Variables	34
No. of Observations	5983
R_{wp}	0.1298
R_p	0.0879
χ^2	1.350

Table S3. Refined atomic parameters for NP Ge.

Atom	**Wyckoff Symbol**	**x**	**y**	**z**	**100*U_{iso} / Å^2**	**Occupancy**
Ge	8a	0.1250	0.1250	0.1250	2.42(2)	1.0

Table S4. Surface area information from N_2 adsorption measurements for NP Ge.

BET Surface Area / m^2 g^{-1}	17.824
Langmuir Surface Area / m^2 g^{-1}	27.944
BJH Adsorption Cumulative Surface Area of Pore between 1.7 – 300.0 nm diameter / m^2 g^{-1}	19.412
BJH Desorption Cumulative Surface Area of Pore between 1.7 – 300.0 nm diameter /m^2 g^{-1}	19.339

Table S5. Indexed lattice planes from the SAED pattern shown in the inset of *Figure 2i.*

Diffraction No.	Indexed Diffraction Distance / nm	Lattice Plane
1	0.327	Ge *(1 1 1)*
2	0.198	Ge *(0 -2 2)*
3	0.167	Ge *(1 3 1)*
4	0.129	Ge *(-1 3 3)*
5	0.114	Ge *(4 2 2)*

Table S6. Volume and porosity information from the 3D tomography analysis of TXM characterisation.

Object total volume (μm^3)	3.91×10^{14}
Volume of closed pores (μm^3)	3.33×10^{10}
Volume of open pores (μm^3)	3.46×10^{14}
Total porosity (%)	88.62

Table S7. Profile fitting of the XPS spectrum shown in *Figure 2m.*

Peak	Peak Position (eV)	Atomic %
Ge *3d5/2* (Ge)	29.26	69.13
Ge *3d3/2* (Ge)	29.88	16.16
Ge *3d* (GeO)	30.9	7.44
Ge *3d* (GeO_2)	32.25	8.27

Table S8. Rietveld refinement results of the Mg_2Ge/MgO powder mixture after the 2nd MW irradiation (*i.e.* following a total irradiation time of 80 s; see also Figure S1).

Chemical Formula	**Mg_2Ge**	**MgO**
Crystal System	Cubic	Cubic
Space Group	*F m -3 m*	*F m -3 m*
Lattice Parameter / Å	6.3985(3)	4.2196(5)
Formula Weight / g mol^{-1}	484.800	161.216
Formula Units, Z	4	4
Calculated Density, ρ / g cm^{-3}	3.073	3.563
Phase fraction / wt.%	51(1)	49(1)
No. of Variables	29	
No. of Observations	2093	
R_{wp}	0.2050	
R_p	0.1456	
χ^2	1.576	

Table S9. Rietveld refinement results of the powder mixture after the 1st MW irradiation of 20 s (see also Figure S2).

Chemical Formula	**Mg_2Ge**	**Mg**	**GeO_2**	**MgO**	**Ge**
Crystal System	Cubic	Hexagonal	Trigonal	Cubic	Cubic
Space Group	*F m -3 m*	*P 63/m m c*	*P 31 2 1*	*F m -3 m*	*F d -3 m*
Lattice Parameter / Å	6.3954(6)	3.2106(3)	4.9931(9)	4.2211(15	5.6579(29)
		3.2106(3)	4.9931(9)	)	
		5.2131(7)	5.6423(15)		
Formula Weight / g mol^{-1}	484.800	48.610	313.764	161.216	580.72
Formula Units, Z	4	2	3	4	8
Calculated Density, ρ / g cm^{-3}	3.078	1.734	4.277	3.560	5.324
Phase fraction / wt.%	37.9(7)	24.3(7)	8.9(4)	28.2(9)	0.7(1)
No. of Variables	34				
No. of Observations	2055				
R_{wp}	0.3249				
R_p	0.2300				
χ^2	1.251				

Table S10. Rietveld refinement results from the Mg_2Ge/MgO sample (originally from 5.5:1 Mg:GeO_2) formed after the thermal de-alloying process and prior to acid washing (see also Figure S7).

Chemical Formula	**MgO**	**Ge**	**Mg_2Ge**
Crystal System	Cubic	Cubic	Cubic
Space Group	*F m -3 m*	*F d -3 m*	*F m -3 m*
Lattice Parameter / Å	4.2150(4)	5.6570(6)	6.3992(14)
Formula Weight / g mol^{-1}	161.216	580.720	484.800
Formula Units, Z	4	8	4
Calculated Density, ρ / g cm^{-3}	3.575	5.327	3.072
Phase fraction / wt.%	73.1(7)	26.1(7)	0.8(2)
No. of Variables		26	
No. of Observations		2082	
R_{wp}		0.2596	
R_p		0.1693	
χ^2		1.357	

References

[1] Fan, Z.; Cappelluti, M.D.; Gregory, D.H. Ultrafast, Energy-Efficient Synthesis of Intermetallics; Microwave-Induced Metal Plasma (MIMP) Synthesis of Mg_2Sn. *ACS Sustain. Chem. Eng*., **2019**, 7, 19686-19698.

[2] Toby, B.H. EXPGUI, a Graphical User Interface for GSAS. *J. Appl. Cryst.* **2001**, 34(2), 210-213.

[3] Cooper, A.S. Precise lattice constants of germanium, aluminum, gallium arsenide, uranium, sulphur, quartz and sapphire. *Acta Crystallogr.*, **1962**, 15, 578-582.

[4] Haines, J.; Cambon, O.; Philippot, E.; Chapon, L.; Hull, S. A neutron diffraction study of the thermal stability of the α-quartz-type structure in germanium dioxide. *J. Solid State Chem.*, **2002**, 166, 434-441.

[5] Grosch, G.H.; Range, K.J. Studies on AB2-type intermetallic compounds, I. Mg_2Ge and Mg_2Sn: single-crystal structure refinement and ab initio calculations. *J. Alloys Compd.*, **1996**, 235, 250-255.

[6] Owen, E.A.; Pickup, L.; Roberts, I.O. Lattice constants of five elements possessing hexagonal structure. *Zeitschrift für Kristallographie-Crystalline Materials*, **1935**, 91, 70-76.

[7] Sasaki, S.; Fujino, K.; Takéuchi, Y. X-ray determination of electron-density distributions in oxides, MgO, MnO, CoO, and NiO, and atomic scattering factors of their constituent atoms. *P. JPN Acad. B-Phys.*, **1979**, 55, 43-48.

[8] Hsieh, C.C.; Lin, Y.G.; Chiang, C. L.; Liu, W.R. Carbon-coated porous Si/C composite anode materials via two-step etching/coating processes for lithium-ion batteries. *Ceram. Int.*, **2020**, 46, 26598-26607.